Check for updates

Vibrating droplet generation to assemble zwitterion-coated gold-graphene oxide stealth nanovesicles for effective pancreatic cancer chemo-phototherapy†

Raj Kumar Thapa,[a] Sae Kwang Ku,[b] Han-Gon Choi,[c] Chul Soon Yong,*[a] Jeong Hoon Byeon [ID] *[d] and Jong Oh Kim*[a]

A vibrating nozzle approach was used to produce uniform (∼2 μm) hybrid droplets containing gold-graphene oxide (Au-GO), doxorubicin (DOX), and zwitterionic chitosan (ZC) for assembly of Au-GO@ZC-DOX stealth nanovesicles (NVs) *via* a single-pass diffusion drying process without any hydrothermal reactions, separations, or purifications. NVs were prepared with a lateral dimension of ∼53.0 nm, a pH-triggered high DOX release profile, and strong photothermal effects. Macrophage opsonization was prevented, resulting in anti-cancer and anti-migration effects, with high intracellular uptake in PANC-1 and MIA PaCa-2 cells. PANC-1 tumor uptake was greater for NVs having the ZC configuration than that for NVs without the ZC configuration, resulting in better anti-tumor effects with minimal toxicities. The vibrating nozzle approach offers significant potential to assemble multi-componential NVs for more efficient anti-tumor treatment and easy user-defined manufacturing of multifunctional nanomedicines.

1 Introduction

The therapeutic relevance of anticancer drugs has been undermined by limitations such as poor biopharmaceutical properties, drug resistance, undefined toxicity, and limited concentrations at the tumor site.[1] Strategies developed to resolve these problems include the use of combinational chemotherapeutics or smarter drug delivery systems.[2] Nano-sized carriers can be exploited for drug delivery *via* leaky tumor vasculature based on the enhanced permeation and retention effect.[3,4] Furthermore, nanoparticles exhibiting external stimuli-responsive behavior offer great potential for hybrid cancer therapeutics. One such potential includes the use of near-infrared (NIR)-sensitive nanoplatforms, with the ability to carry anticancer agents and induce photothermal effects resulting in tumor regression.[5] Chemo-phototherapies that combine doxorubicin (DOX), as a chemotherapeutic agent, and gold nano-particle (AuNP)-decorated graphene oxide (GO), as a photothermal agent, have been intensively studied. These studies mostly use multistep hydrothermal reactions, separations, and purifications to functionalize Au and GO surfaces to incorporate DOX.[6–8]

GO is a two-dimensional carbon allotrope that possesses several unique and advantageous properties, including a large surface area for drug adsorption and the ability to absorb NIR, which enables it to exert photothermal effects.[9,10] Furthermore, GO can be utilized alone or in combination with other functional components and/or bioactive molecules. The combination of AuNPs and GO has provided a viable approach based on their high drug-loading capacities, excellent biocompatibilities, and NIR-induced photothermal conversion efficacy.[11,12] AuNPs also exhibit a high absorption capability for converting NIR to heat, which can be used for localized hyperthermia.[13,14] Studies using AuNP-decorated GO (Au-GO) have presented excellent photothermal effects that can be manipulated by altering the density and size of the AuNPs.[15,16] Furthermore, GO provides a large surface area for DOX-loading based on π–π interactions,[17] resulting in high drug loading for enhanced tumor delivery.

Nanocarriers with a cationic surface charge (*e.g.*, Au-GO incorporated with DOX [Au-GO@DOX]) can easily enter cells, attributable to their adsorptive interactions with the cell membranes.[18,19] However, these nanocarriers are easily cleared from the body by means of the reticuloendothelial

[a]*College of Pharmacy, Yeungnam University, Gyeongsan 38541, Republic of Korea.*
E-mail: csyong@yu.ac.kr, jongohkim@yu.ac.kr
[b]*College of Korean Medicine, Daegu Haany University, Gyeongsan 38610,*
Republic of Korea
[c]*College of Pharmacy, Institute of Pharmaceutical Science and Technology,*
Hanyang University, Ansan 15588, Republic of Korea
[d]*School of Mechanical Engineering, Yeungnam University, Gyeongsan 38541,*
Republic of Korea. E-mail: postjb@yu.ac.kr
†Electronic supplementary information (ESI) available. See DOI: 10.1039/
c7nr07603g

system, leading to compromised drug delivery to the target site.[20] To avoid this problem, nanocarriers are often stealth-coated with polyethylene glycol (PEG).[21] However, previous reports suggest that the presence of PEG limits interactions between the carriers and the target cells.[22,23] Therefore, development of removable stealth coatings that remain intact during circulation and can be removed once the target site is reached has become a challenging issue. The acidic pH observed in tumor sites can be utilized to remove the stealth coating from the nanocarriers, which enables interactions with cancer cells.[24,25] Zwitterionic chitosan (ZC) derivatives can be used as stealth-coatings for nanocarriers, as they are biocompatible and inhibit opsonization, attributable to the zwitterionic character (*i.e.*, totally neutral potential under physiological conditions),[26] resulting from the amidation of the primary chitosan amines with succinic anhydride.[27]

To assemble stealth-coated multifunctional nanocarriers, the present study used a vibrating nozzle approach to efficiently produce hybrid droplets containing Au-GO, DOX, and ZC that were subsequently solvent extracted to assemble Au-GO@ZC-DOX stealth nanovesicles (NVs). These NVs were then evaluated for their potential *in vitro* and *in vivo* chemo-phototherapeutic effects in pancreatic cancer cells.

2 Materials and methods

2.1 Materials

Graphite (C-072561) and gold (AU-172561) rods were obtained from Nilaco Corporation (Tokyo, Japan). DOX was a gift from Dong-A Pharmaceutical Company (Yongin, South Korea). Potassium permanganate ($KMnO_4$) and FITC were purchased from Sigma-Aldrich (St Louis, MO, USA). Lysotracker green was purchased from Thermo Fischer Scientific Inc. (Waltham, MA, USA). PANC-1 and MIA PaCa-2 cancer cells were obtained from the Korean Cell Line Bank (Seoul, South Korea). All other chemicals were of reagent grade and used without further purification.

2.2 Preparation of Au-GO@ZC-DOX

Au-GO flakes were first prepared based on a previous report.[28] The flakes were then dispersed in deionized water (0.7 mg mL^{-1}) with ZC (0.1 mg mL^{-1}) and DOX (0.2 mg mL^{-1}). The ZC adopted in this study is identical to a previous report,[29] and the molar ratio of succinic anhydride to chitosan amine (An/Am ratio) is 0.7. The optimum amount of ZC was confirmed *via* a trial-and-error approach with scanning mobility particle sizer (SMPS, 3936, TSI, USA) measurements (Fig. S1, ESI†). The dispersion was connected to a vibrating (128 kHz) nozzle and it formed hybrid droplets after passing through the nozzle. The solvent was extracted from the droplets in a diffusion dryer to form Au-GO@ZC-DOX NVs, which were subsequently collected on a polished cylindrical aluminum rod. The NV-collected rod was then immersed in PBS to release the NVs for *in vitro* and *in vivo* experiments.

2.3 Characterization

2.3.1 Physicochemical properties of Au-GO@DOX and Au-GO@ZC-DOX. The geometric mean diameters for Au-GO, Au-GO@DOX, and Au-GO@ZC-DOX were determined using a SMPS (3936, TSI Inc., USA). Light absorption properties were further analyzed using a UV-vis spectrophotometer (T60, PG Instruments, UK). TEM (CM-100, FEI/Philips, USA) was performed for the morphological analysis of the prepared Au-GO, Au-GO@DOX, and Au-GO@ZC-DOX. The prepared samples were loaded onto a carbon-coated copper grid and dried under particle-free atmospheric conditions for TEM analysis.

2.3.2 *In vitro* drug release. The *in vitro* release profiles of DOX from Au-GO@ZC-DOX were measured using the dialysis method. Briefly, the desired volumes of Au-GO@ZC-DOX were placed into a dialysis membrane tubing (Spectra/Por, MWCO 3500 Da, USA), and immersed in 30 mL of either PBS (pH 7.4) or ABS (pH 5.0). The tubing was maintained at 37 °C and 100 rpm, and the samples were withdrawn at predetermined time intervals. The amount of DOX released was quantified using a high-performance liquid chromatography (HPLC) system (Hitachi, Japan) comprising an L-2130 pump, an L-2200 auto-sampler, an L-2420 UV-vis detector, and an L-2350 column oven with Ezchrom Elite software (318a, Japan). An Inertsil C_{18} column (150 mm × 4.6 mm, 5 μm particle size, Cosmosil, NacalaiTesque Inc., USA) was used to perform isocratic elution with a mobile phase consisting of methanol : acetonitrile : acetic acid (1%) at a ratio of 50 : 49 : 1 (v/v/v), a flow rate of 1.0 mL min^{-1}, and a column temperature of 25 °C. Each 20 μL sample was injected for analysis, and UV absorbance was measured at a wavelength of 254 nm.

2.3.3 NIR-induced photothermal effects. Increasing temperatures following exposure to Au-GO, Au-GO@DOX, and Au-GO@ZC-DOX under 808 nm NIR laser irradiation (3.0 W cm^{-2}) were digitally evaluated using a thermal camera (Therm-App TH, Israel).

2.4 Biological assessments

2.4.1 Cell viability assay. The *in vitro* cell viability of PANC-1 and MIA PaCa-2 cells was determined using the 3-(4,5-dimethylthiazol-2-yl)-5-(3-carboxymethoxyphenyl)-2-(4-sulfophenyl)-2*H*-tetrazolium (MTS) assay (Promega, USA). Pancreatic cancer cells (1 × 10^4 cells per well) were seeded in 96-well plates and treated with DOX, Au-GO, Au-GO@ZC, Au-GO@DOX, and Au-GO@ZC-DOX with or without 808 nm NIR laser exposure. Following treatment for 24 h, the MTS solution was added to each well, allowing the color to develop. The absorbance was then measured at 493 nm using a microplate reader (Multiskan EX, Thermo Scientific, USA) to determine cell viabilities.

2.4.2 Cellular uptake study

FACS analysis. PANC-1 and MIA PaCa-2 cells (1 × 10^5 cells per well) were seeded in 6-well plates, incubated overnight at 37 °C, and treated with Au-GO@ZC-DOX, with replicates constructed by varying drug concentration and incubation time to determine concentration- and time-dependent cellular uptake.

After incubating for suitable amounts of time, the cells were washed twice with cold PBS, detached using trypsin, and centrifuged and washed to obtain a cell pellet, which was redispersed in 1 mL cold PBS. FACS analysis for the quantitative determination of cellular uptake in various groups was performed using a BD FACS Verse flow cytometer (BD Biosciences, San Jose, CA, USA). Untreated cells served as the control.

Fluorescence microscopy. PANC-1 and MIA PaCa-2 cells (2×10^4 cells per well) were seeded on coverslips placed on 12-well plates, incubated for 24 h, and treated with Au-GO@ZC-DOX for 1 h. LysoTracker green was used to track lysosomes within the cells. The final concentrations of DOX and LysoTracker green were 1 μg mL^{-1} and 100 ng mL^{-1}, respectively. Finally, the cells were washed with PBS, fixed in 4% paraformaldehyde, and mounted on glass slides for observation using a confocal laser scanning microscope (CLSM, Leica Microsystems, Wetzlar, Germany).

2.4.3 Apoptosis assay. Pancreatic cancer cells (1×10^5 cells per well) were seeded in a 12-well plate, incubated for 24 h, and then treated with DOX, Au-GO, Au-GO@ZC, Au-GO@DOX, and Au-GO@ZC-DOX with or without 808 nm NIR laser exposure. After 24 h, the cells were harvested using trypsin, centrifuged, and washed with PBS. The resulting cell pellet was mixed with a binding buffer and stained with PE-annexin V and 7-amino actinomycin D (7-AAD) for 10 min. The cells were finally diluted with the binding buffer and analyzed on a BD FACS Verse flow cytometer (BD Biosciences, San Jose, CA, USA). Untreated cells served as the control.

2.4.4 Cell migration assay. Cell migration was analyzed in pancreatic cancer cells using a transwell assay. PANC-1 and MIA PaCa-2 cells were separately treated with DOX, Au-GO@DOX, and Au-GO@ZC-DOX for 6 h. Afterwards, the cells were collected and 100 μL of the cell suspension (5×10^5 cells per mL, prepared with serum-free medium) was seeded onto collagen-coated inserts (0.8 μm; BD Bioscience). The inserts were placed into wells containing 10% fetal bovine serum (FBS) in Dulbecco's modified Eagle's medium (DMEM), and cell migration was measured. Following a 12 h incubation, the migrated cells were fixed, stained with 0.5% crystal violet, and photographed using a microscope. For quantification, the dye from the insert membrane was dissolved in acetic acid, and the absorbance was measured using a UV-vis spectrophotometer at λ_{max} = 470 nm. The inhibition of cell migration was calculated using the following formula:

$$\text{Inhibition (\%)} = \frac{\text{OD}_{control} - \text{OD}_{sample}}{\text{OD}_{control}} \times 100 \qquad (1)$$

where OD$_{control}$ and OD$_{sample}$ refer to the optical densities of the control and samples, respectively.

2.4.5 *In vitro* cellular uptake of Au-GO and Au-GO@ZC in RAW 264.7 macrophages. The cellular uptake of Au-GO@FITC and Au-GO@ZC-FITC was evaluated in RAW 264.7 macrophages. The macrophages were seeded in 12-well plates and treated with Au-GO@FITC and Au-GO@ZC-FITC for 1 h. Qualitative uptake was determined *via* a confocal microscope

and quantitative uptake was determined *via* FACS analysis, as previously described.

2.4.6 *In vivo* antitumor study

Development of PANC-1 tumor xenograft models. Six-week old female BALB/c nude mice were subcutaneously injected with 1×10^7 PANC-1 cells dispersed in 100 μL serum-free DMEM in the right thigh flank. Once the tumor sizes reached ~100 mm^3, the mice were randomly divided into 6 groups (n = 6 per group). All animal procedures were performed in accordance with the Guidelines for Care and Use of Laboratory Animals of Yeungnam University and approved by the Animal Ethics Committee of Yeungnam University.

Drug/formulation treatment and data collection. Xenograft mouse models were subjected to intravenous administration of DOX, Au-GO@DOX, Au-GO@DOX + NIR, Au-GO@ZC-DOX, and Au-GO@ZC-DOX + NIR through the tail vein. One group was left untreated, serving as the control. A treatment dose equivalent to 2.5 mg drug per kg mouse body weight was administered on days 0, 4, 8, and 12. Body weight and tumor dimensions of the mice were recorded. Tumor volumes were calculated using the formula:

$$\text{Tumor volume} = \frac{1}{2} \times (\text{length}) \times (\text{breadth})^2. \qquad (2)$$

Histopathological examination. Upon completion of the study period, representative tumor masses from the xenograft mouse model were removed from euthanized mice and fixed in formalin for further studies. Histopathological and histomorphometric changes of the tumor masses were observed using hematoxylin and eosin staining. Additionally, tumor cell apoptosis (caspase-3 and cleaved-PARP), angiogenesis [CD31/platelet endothelial cell adhesion molecule 1 (PECAM-1)], and proliferation (Ki-67) were determined using immunohistochemical staining with primary antisera and avidin–biotin–peroxidase complex (ABC). Changes in tumor cell volumes, caspase-3, PARP, CD31, and Ki-67 expression following treatment with different formulations were calculated.

2.5 Statistical analysis

Results are expressed as the mean ± standard deviation (SD). Student's *t*-test (for pairs of groups) and one-way ANOVA (for multiple groups) were used to determine statistical differences. $P < 0.05$ was considered statistically significant.

3 Results and discussion

NVs containing AuNPs were deliberately fabricated to induce strong plasmonic coupling between the AuNPs, thus introducing enhanced localized surface plasmon resonance absorption for effective NIR-induced photothermal therapy.[27] Nanoformulation assembly *via* solvent extraction has commonly been attempted with high-pressure spraying devices to produce droplets containing the desired solutes by passing them through a nozzle/orifice. Even though a spraying device was previously shown to be suitable for producing multi-com-

ponential nanocarriers,[27] significant pressure differences before and after the nozzle/orifice resulted in the disassembly of the AuNPs and GO@ZC-DOX (Fig. S2, ESI†). Hybrid droplets (~2 μm) are generated when perforated stainless-steel plates (placed in the bottom of a precursor solution bottle) are vibrated at 128 kHz, allowing the solution (Au-GO, DOX, and ZC in water) to pass through the plate. The droplets are carried by a N_2 gas flow into a pin (+4 kV)-to-ring (ground) field charger to positively charge the droplets (*i.e.*, give repulsive forces between the droplets to prevent agglomeration). Subsequently, the solvent from the droplets is extracted in a diffusion dryer to form the NVs (Fig. S2, ESI†) in a single-pass configuration (Fig. 1).

The feasibility of the vibrating nozzle approach for assembling nano-sized vesicular structures was first validated *via* size distribution measurements in an aerosol state after solvent extraction. Distributions of Au-GO, Au-GO@DOX, and Au-GO@ZC-DOX were determined using the SMPS (Fig. 2A); their geometric mean diameters were 27.5 ± 1.4, 39.6 ± 1.5, and 53.6 ± 1.6 nm, respectively. Deposition of DOX on Au-GO led to an increase in size for the Au-GO@DOX configuration. The addition of ZC molecules onto Au-GO@DOX resulted in a further increase in size for the Au-GO@ZC-DOX configuration. The various forms (*i.e.*, Au-GO@DOX and Au-GO@ZC-DOX) showed unimodal distributions similar to that of Au-GO alone, implying that nearly all the Au-GO was covered by DOX or ZC-DOX during the vibrating droplet generation and the subsequent diffusion drying process. The geometric standard deviation (GSD) of Au-GO@ZC-DOX was 1.61 (close to quasi-
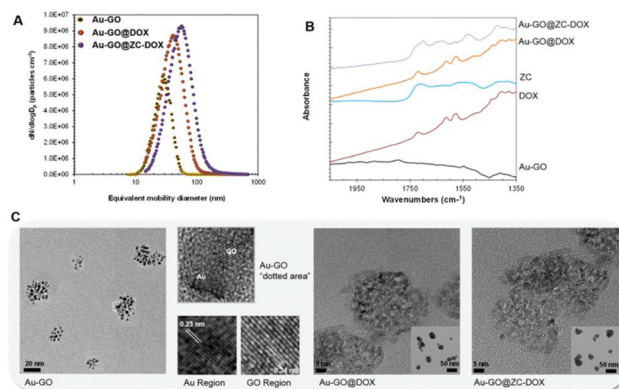

Fig. 2 (A) Size distributions of gold-graphene oxide (Au-GO) (without doxorubicin [DOX] or zwitterionic chitosan [ZC]-DOX solution), Au-GO@DOX (DOX dissolved in water), and Au-GO@ZC-DOX (ZC-DOX dissolved in water) after solvent extraction in a diffusion dryer. (B) Fourier transform infrared (FTIR) spectra from absorbance measurements of samples on polytetrafluoroethylene substrates (adopted as a reference material for the measurements) are shown. (C) Low- and high-magnification transmission electron microscopy (TEM) images of Au-GO, Au-GO@DOX, and Au-GO@ZC-DOX are shown. Specimens were prepared by direct aerosol sampling after a diffusion drying process in a single-pass configuration.
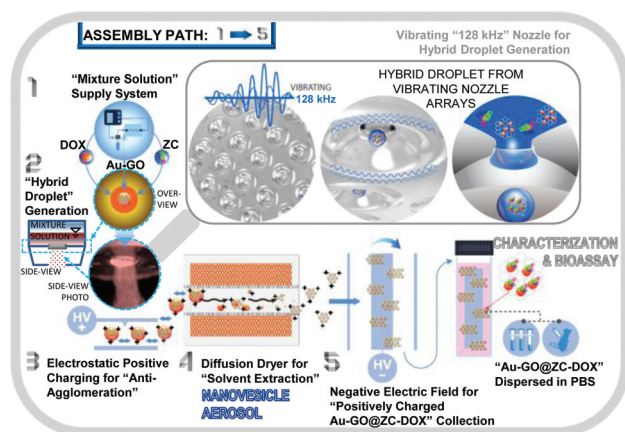
monodisperse distribution, 1.15–150), although the diffusion coefficient of particles in gas is larger by three orders of magnitude than those in the aqueous phase. This is even better than that in a previous report (1.72)[30] that is only concerned with lateral nanodimensional GO and DOX, which may be due to uniform droplet generation to be dried *via* the vibrating nozzle system. The average zeta potentials of Au-GO, Au-GO@DOX, and Au-GO@ZC-DOX were −5.4, +10.2, and +1.4 mV, respectively. Loading of DOX onto the Au-GO surface resulted in the development of a positive potential, which was then neutralized by adding ZC, attributable to its zwitterionic nature.[29] We performed a Fourier transform infrared (FTIR, iS-10, Thermo Electron, USA) analysis (Fig. 2B), and the characteristic peaks at 1400 and 1735 cm^{-1} corresponded to C–O bending and C=O stretching of the GO carboxyl groups, respectively.[31] DOX presented characteristic peaks at 1600 and 1735 cm^{-1}, whereas ZC presented broad peaks from 1500–1750 cm^{-1}. When DOX was loaded onto Au-GO, the characteristic peaks of DOX were prominent, suggesting the successful formation of Au-GO@DOX. Upon addition of ZC onto the Au-GO@DOX, the characteristic peaks of DOX were reduced and those of ZC were prominent, implying the successful formation of Au-GO@ZC-DOX. A morphological analysis of Au-GO, Au-GO@DOX, and Au-GO@ZC-DOX was performed using transmission electron microscopy (TEM, CM-100, FEI/Philips, USA) (Fig. 2C). Au-GO particles were observed to be of uniform size, as suggested by the particle size analysis. A high-magnification TEM image showed AuNP deposition on the GO sheets, as presented by the lattice fringes with an interplanar distance of 0.23 nm corresponding to the (111) AuNP planes.[32] Furthermore, GO presented lattice

Fig. 1 Schematic of gold-graphene oxide (Au-GO), doxorubicin (DOX), and zwitterionic chitosan (ZC; Au-GO@ZC-DOX) nanovesicles (NVs) assembled *via* a vibrating (128 kHz) nozzle approach. Au-GO was first dispersed in deionized water with DOX and ZC (step 1), and then filled in a bottle connected with a vibrating nozzle to produce hybrid droplets (step 2). The generated droplets were electrostatically positively charged (step 3) and passed through a diffusion dryer to remove the solvent from the droplets and form Au-GO@ZC-DOX NVs (step 4). The NVs were collected on a polished aluminum rod with a negative electric field (step 5); the rod was immersed in phosphate-buffered saline (PBS) to detach the NVs for the preparation of the dispersion to be employed for physico-chemical characterization and *in vitro* and *in vivo* bioassays.

fringes with an interplanar distance of 0.34 nm, as suggested in a previous study.[33] Increments in the lateral dimensions of Au-GO@DOX and Au-GO@ZC-DOX were clearly visible from the TEM observations, proving that the loading of DOX and ZC-DOX without Au-GO or AuNP divisions was successful.

Digital images of Au-GO, Au-GO@DOX, and Au-GO@ZC-DOX are presented in the insets of ultraviolet-visible (UV-vis) spectra (Fig. 3A). A single-pass loading of DOX onto Au-GO was confirmed *via* the bright red color shown in the digital image. ZC covering of Au-GO@ZC led to a reduction in the color intensity for Au-GO, attributable to the appropriate coating of the NVs. Even though the incorporation of DOX or ZC-DOX induced a shoulder peak at around 500 nm, the UV-vis spectra for Au-GO@DOX and Au-GO@ZC-DOX showed broadband light absorption characteristics suitable for NIR-induced photothermal effects.

The *in vitro* drug release profiles of DOX from Au-GO@ZC-DOX were determined under different pH conditions (Fig. 3B). The mass fraction of DOX in Au-GO@ZC-DOX was measured using a piezobalance particle monitor (3522, Kanomax, Japan) to be approximately 0.2, which is consistent with the DOX content in the mixture solution. This may be due to direct drying of the solution after vibrating droplet

generation without separation or purification. A significant increase in DOX release under acidic pH was evident. Tumor microenvironments possess acidic conditions[34] that favor the enhanced release of DOX within the cancer cells. Chitosan is highly soluble in acidic pH,[35] which might potentiate uncovering of the ZC layer from Au-GO@ZC-DOX and subsequent DOX release. Furthermore, DOX protonation in an acidic microenvironment may result in a more hydrophilic form that enhances the drug release profiles.[36] DOX released from Au-GO@ZC-DOX was also determined in the presence of NIR laser irradiation at 1, 3, and 6 h. An abrupt DOX release profile can be attributed to elevations in temperature caused by the NIR laser irradiation of Au-GO, possibly resulting in enhanced ZC and DOX solubility in the acidic media.[37] The photothermal effects of Au-GO, Au-GO@ZC, and Au-GO@ZC-DOX were evaluated using a thermal camera (Fig. 3C). Upon 808 nm NIR laser irradiation of GO, light absorption to heat conversion was mediated by energy transfer from the π-network restoration, resulting in increased temperature.[38] Furthermore, AuNPs can generate heat upon NIR irradiation *via* the surface plasmon resonance (SPR) effect or electron vibrations.[39] Thermal elevations observed for Au-GO under NIR laser irradiation led to a local temperature of approximately 57 °C. DOX loading slightly reduced the photothermal capacity, attributable to the disturbance resulting from the NIR-laser irradiated coverage of the Au-GO surfaces. Similar patterns of photothermal elevations were observed with Au-GO@ZC-DOX, suggesting that photothermal effects are suitable in combination with DOX for inducing potent anticancer effects.

Cellular uptake of Au-GO@ZC-DOX was qualitatively and quantitatively evaluated in PANC-1 and MIA PaCa-2 cells. Confocal images of the treated cells are presented in Fig. 4A. High cellular uptake was evident in both cell lines, as shown by the intense red staining within the cells. The uptake mechanism was further elucidated using LysoTracker green. According to the results, NVs were mostly concentrated within
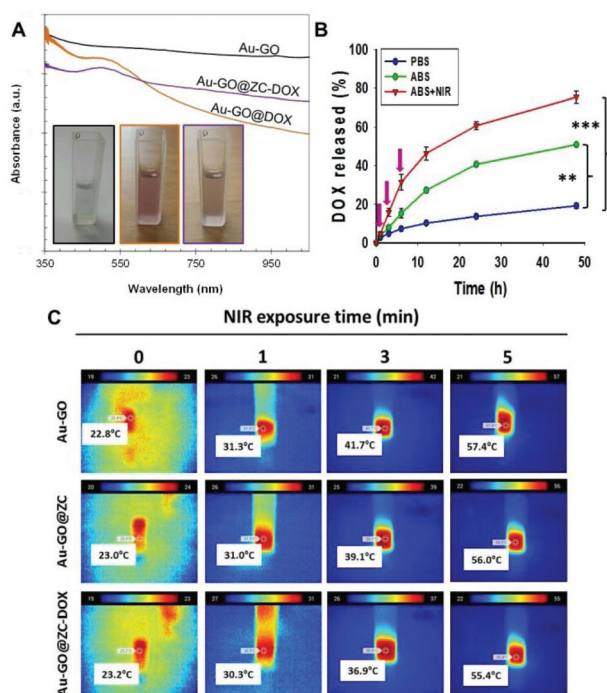

Fig. 3 (A) Ultraviolet-visible (UV-vis) spectra of gold-graphene oxide (Au-GO), Au-GO with doxorubicin (Au-GO@DOX), and Au-GO@DOX coated with zwitterionic chitosan (Au-GO@ZC-DOZ), including photographs of the dispersions, are shown. (B) *In vitro* drug release profiles of DOX from Au-GO@ZC-DOX in phosphate-buffered saline (PBS, pH 7.4) and acetate-buffered saline (ABS, pH 5.0) are shown. Arrows indicate near-infrared (NIR) laser irradiation for 5 min at 1-, 3-, and 6 h time points (**$P < 0.01$, ***$P < 0.001$). (C) NIR-induced photothermal effects of Au-GO, Au-GO@ZC, and Au-GO@ZC-DOX are shown (NIR exposure conditions: 808 nm, 3.0 W cm^{-2}, 5 min).
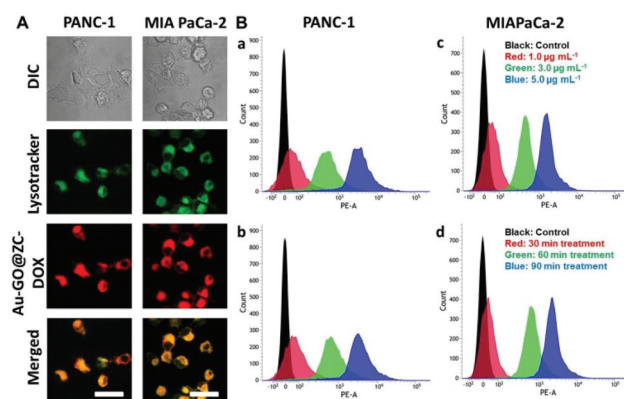

Fig. 4 Cellular uptake study of gold-graphene oxide (Au-GO), doxorubicin (DOX), and zwitterionic chitosan (Au-GO@ZC-DOX) nanovesicles in PANC-1 and MIA PaCa-2 cells. (A) Confocal images and (B) fluorescence-activated cell sorting (FACS) analysis [(a, c) concentration- and (b, d) time-dependent uptake (scale bar = 50 μm)] are shown.

the cell lysosomes following endocytosis. A quantitative evaluation of the cellular uptake in pancreatic cancer cells is presented in Fig. 4B. Both cell lines presented concentration- and time-dependent cellular uptake. Cytotoxicity in PANC-1 and MIA PaCa-2 cells following treatments with DOX, Au-GO, Au-GO@ZC, Au-GO@DOX, and Au-GO@ZC-DOX with or without NIR laser irradiation is presented in Fig. S3 (ESI†). Treatment with DOX resulted in a concentration-dependent anticancer effect based on its ability to intercalate with DNA and disrupt topoisomerase-II-mediated DNA repair.[40] Au-GO and Au-GO@ZC caused a slight increase in cytotoxicity, which was further enhanced with NIR laser irradiation, attributable to the photothermal effects of Au-GO.[38,39] There were no significant differences in cell viabilities between the Au-GO@DOX and Au-GO@ZC-DOX treatments. NVs were significantly taken up by lysosomes (acidic pH, suitable for solubilizing the condensed ZC layer that could then release DOX for delivery to the nucleus), which enabled the ZC layer to be easily uncovered for efficient drug release within the cells and enhanced cytotoxic effects, as demonstrated by the confocal image analyses.

Induction of cellular apoptosis in PANC-1 and MIA PaCa-2 cells was evaluated *via* fluorescence-activated cell sorting (FACS) (Fig. S4, ESI†). Au-GO and Au-GO@ZC did not significantly induce apoptosis; however, 808 nm NIR laser irradiation increased the number of apoptotic cells in the PANC-1 and MIA PaCa-2 cell lines. A similar pattern of apoptosis was demonstrated in cells treated with DOX, Au-GO@DOX, and Au-GO@ZC-DOX, attributable to the successful intake of NVs within the cells. NIR-laser irradiation further enhanced the number of apoptotic cells, owing to combinational effects (*i.e.*, chemotherapeutic and photothermal effects). The inhibition of PANC-1 and MIA PaCa-2 cell migration was studied using a transwell assay (Fig. S5, ESI†). Both pancreatic cancer cell lines possess high potential for *in vivo* cell migration by means of the epithelial mesenchymal transition, resulting in higher metastatic rates.[40] Following treatment with DOX, Au-GO@DOX, and Au-GO@ZC-DOX, there were significant reductions in the ability of pancreatic cancer cells to migrate. The final formulation, Au-GO@ZC-DOX, presented the highest anti-migration effects, which could be highly beneficial for preventing metastasis and prolonging lifespan.[41]

The protective ability of ZC to enhance NV blood circulation time and prevent opsonization was studied using RAW 264.7 macrophages (Fig. S6, ESI†). Au-Go loaded with fluorescein-5(6)-isothiocyanate (Au-GO@FITC) was extensively taken up by the macrophages, while the uptake of Au-GO@ZC-FITC was not significant. Both confocal imaging and FACS analysis were consistent with these results. The addition of the ZC layer maintained the neutral charge of the NVs, thus preventing opsonization.[35] These effects were highly beneficial for extending the blood circulation time of Au-GO@ZC-DOX, thereby enabling it to reach the tumor site more efficiently.

The *in vivo* biodistribution of intravenously injected Cy5.5-loaded Au-GO (*i.e.*, Au-GO@Cy5.5) and Au-GO@ZC (*i.e.*, Au-GO@ZC-Cy5.5) was evaluated (Fig. 5). Considering the fluo-
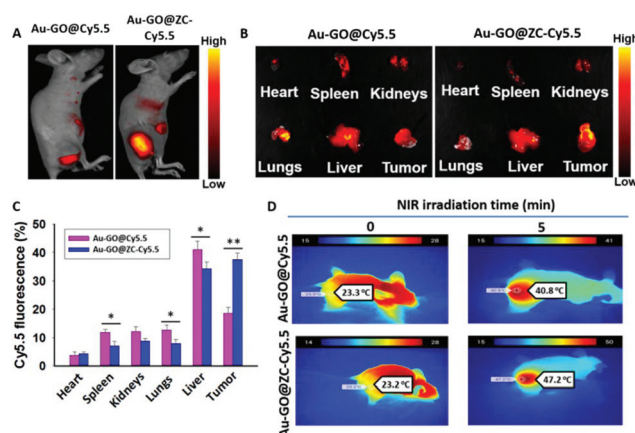

Fig. 5 (A) *In vivo* biodistribution of Cy5.5-loaded gold-graphene oxide (Au-GO) nanovesicles with (*i.e.*, Au-GO@ZC-Cy5.5) and without (*i.e.*, Au-GO@Cy5.5) a zwitterionic chitosan (ZC) coating in PANC-1 tumor xenograft mice. (B) Imaging and (C) quantification of Cy5.5-loaded Au-GO and Au-GO@ZC distributions in different organs following intravenous administration are shown (*P < 0.05; **P < 0.01). (D) Images for near infrared (NIR) laser-induced *in vivo* photothermal effects in tumors pretreated with Au-GO@Cy5.5 and Au-GO@ZC-Cy5.5 (NIR exposure conditions: 808 nm, 3.0 W cm^{-2}, 5 min) are shown.

rescence quenching effect of DOX by Au-GO, the same quantities of Cy5.5 were employed instead of DOX for the biodistribution measurements. A remarkable difference in the uptake between Au-GO@Cy5.5 and Au-GO@ZC-Cy5.5 in tumors and organs was detected. The uptake of Au-GO@ZC-Cy5.5 was significantly higher than that of Au-GO@Cy5.5 in treated PANC-1 tumors (Fig. 5A). This may be due to the solid phase of ZC at normal physiological pH that can minimize DOX leakage during blood circulation as well as maintain the NV integrity until delivery to the tumor sites. Furthermore, the uptake of Au-GO@ZC-Cy5.5 in different organs was significantly lower than that of Au-GO@Cy5.5 (Fig. 5B and C), attributable to ZC-attenuated opsonization, which allowed longer circulation times for the delivery of Au-GO@ZC-Cy5.5 to tumors. Macrophages are abundant in organs (liver, lungs, spleen, and kidneys);[42] thus, opsonization by macrophages in these organs led to extensive accumulation of Au-GO@Cy5.5. In contrast, Au-GO@ZC-Cy5.5 was minimally distributed. The photothermal effects of the treated xenograft tumors were also validated *in vivo* (Fig. 5D). According to the biodistribution studies, Au-GO@ZC-Cy5.5 accumulation was higher in PANC-1 xenograft tumors, which led to better photothermal effects than those of Au-GO@Cy5.5. High temperatures (41 °C) enhance blood perfusion and blood vessel dilation, triggering a heat-shock response for repair and protection of cells from thermal injury.[43] Furthermore, higher temperatures (46–52 °C) cause cell death *via* ischemia, microvascular thrombosis, and hypoxia,[44] implying that photothermal ablation of Au-GO@ZC-Cy5.5 may be suitable for controlled and enhanced anti-tumor effects.

In vivo antitumor effects were evaluated in a PANC-1 xenograft mouse model (Fig. 6A). Treatment with DOX presented
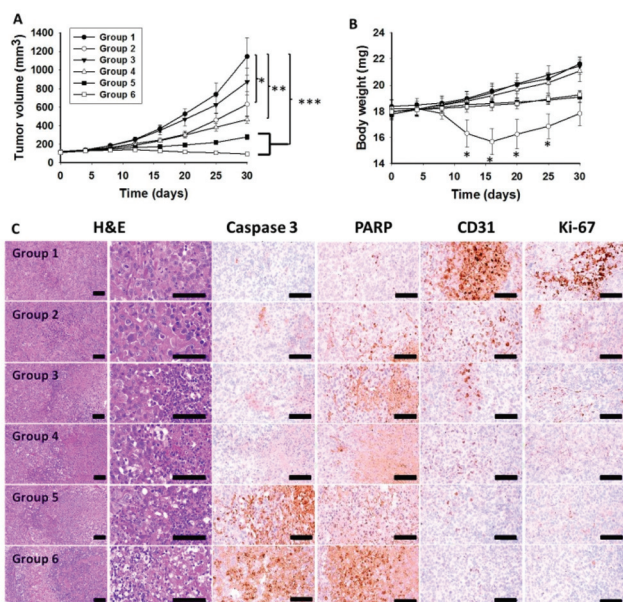
Fig. 6 *In vivo* antitumor study showing changes in (A) tumor volumes and (B) body weights of PANC-1 xenograft mice following treatments (*$P < 0.05$, **$P < 0.01$, ***$P < 0.001$). (C) Immunohistochemical evaluation of PANC-1 xenograft tumors in mice from different treatment groups is shown. Group 1: Control, Group 2: doxorubicin (DOX), Group 3: gold-graphene oxide and doxorubicin (Au-GO@DOX) nanovesicles, Group 4: Au-GO@DOX plus near infrared irradiation (Au-GO@DOX + NIR) nanovesicles, Group 5: Au-GO@-DOX loaded with zwitterionic chitosan (Au-GO@ZC-DOX) nanovesicles, and Group 6: Au-GO@ZC-DOX + NIR (NIR exposure conditions: 808 nm, 3.0 W cm^{-1}, 5 min). Changes in the level of caspase-3, poly ADP ribose polymerase (PARP), CD-31, and Ki-67 expression in tumor cells from treated groups are shown (scale bars: 120 μm).

better antitumor effects than those with Au-GO@DOX, likely attributable to Au-GO@DOX being easily opsonized by macrophages. Following NIR irradiation to Au-GO@DOX-treated mice, the antitumor effects improved as a result of the combinational (*i.e.*, chemo- and photothermal-therapies) therapeutic effects for tumor ablation. A significant reduction in the PANC-1 tumor volume was achieved following the treatment with Au-GO@ZC-DOX, which was further reduced by NIR-laser irradiation to tumors. Unlike *in vitro* assays, this enhanced antitumor activity was probably due to different DOX diffusions into the three-dimensional tumor sites. The NIR irradiation may help in the insufficient release of DOX to deactivate cancer cells through photothermal killing. Changes in body weight were assessed after the treatments to further evaluate the toxicity. Following treatment with DOX, significant reductions in body weights were observed in the mice (Fig. 6B); this phenomenon might be attributable to DOX being easily distributed throughout the body, which causes severe adverse effects, including cardiotoxicity.[45] However, at the end of the study period, the body weights had returned to normal, likely attributable to a reversal of the adverse effects. There were no significant changes in body weights for all other treatment groups, suggesting their suitability for *in vivo*

studies. Organ toxicities following treatments were also determined (Fig. S7, ESI†), with no abnormal findings in the tested organs (heart, liver, lung, kidney, and spleen) for all treatments. These results thus confirm the suitability of Au-GO@ZC-DOX for *in vivo* antitumor studies. Finally, tumor immunohistological analyses were conducted (Fig. 6C). Markers of apoptosis (caspase-3 and poly ADP ribose polymerase [PARP]) were significantly increased, while markers of proliferation (Ki-67) and angiogenesis (CD-31) were significantly reduced for the Au-GO@ZC-DOX + NIR configuration, suggesting efficient anticancer effects against pancreatic cancer. This encourages combined therapies with advanced electronics to secure localized photoinduced therapies for safer and more efficient cancer treatments.[46]

4 Conclusions

In conclusion, we developed lateral nanodimensional (~53.0 nm) zwitterion-coated Au-GO@ZC-DOX stealth NVs *via* a vibrating nozzle approach that showed acidic microenvironment-responsive DOX release profiles. Enhanced cellular uptake, cytotoxicity, and anti-migration effects of Au-GO@ZC-DOX were successfully demonstrated in pancreatic cancer cells (PANC-1 and MIA PaCa-2). Furthermore, *in vivo* biodistribution and anti-tumor effects resulting from the chemo-photo-therapeutic properties of the NVs were promising in a PANC-1 xenograft mouse model. Potent anticancer effects, minimal opsonization, and reduced toxicity suggest that the NVs are an effective formulation for pancreatic cancer treatment; thus, the vibrating nozzle approach demonstrates great potential for efficient built-to-order manufacturing of multifunctional nanotherapeutic applications.

Conflicts of interest

There are no conflicts to declare.

Acknowledgements

Notes and references

1 S. Guo, L. Lv, Y. Shen, Z. Hu, Q. He and X. Chen, *Sci. Rep.*, 2016, **6**, 21459.
2 D. Liu, F. Yang, F. Xiong and N. Gu, *Theranostics*, 2016, **6**, 1306.
3 B. Chen, W. Dai, B. He, H. Zhang, X. Wang, Y. Wang and Q. Zhang, *Theranostics*, 2017, **7**, 538.

4 B. Pelaz, C. Alexiou, R. A. Alvarez-Puebla, F. Alves, A. M. Andrews, S. Ashraf, L. P. Balogh, L. Ballerini, A. Bestetti, C. Brendel, S. Bosi, M. Carril, W. C. W. Chan, C. Chen, X. Chen, X. Chen, Z. Cheng, D. Cui, J. Du, C. Dullin, A. Escudero, N. Feliu, M. Gao, M. George, Y. Gogotsi, A. Grünweller, Z. Gu, N. J. Halas, N. Hampp, R. K. Hartmann, M. C. Hersam, P. Hunziker, J. Jian, X. Jiang, P. Jungebluth, P. Kadhiresan, K. Kataoka, A. Khademhosseini, J. Kopeček, N. A. Kotov, H. F. Krug, D. S. Lee, C.-M. Lehr, K. W. Leong, X.-J. Liang, M. Ling Lim, L. M. Liz-Marzán, X. Ma, P. Macchiarini, H. Meng, H. Möhwald, P. Mulvaney, A. E. Nel, S. Nie, P. Nordlander, T. Okano, J. Oliveira, T. H. Park, R. M. Penner, M. Prato, V. Puntes, V. M. Rotello, A. Samarakoon, R. E. Schaak, Y. Shen, S. Sjöqvist, A. G. Skirtach, M. G. Soliman, M. M. Stevens, H.-W. Sung, B. Z. Tang, R. Tietze, B. N. Udugama, J. S. VanEpps, T. Weil, P. S. Weiss, I. Willner, Y. Wu, L. Yang, Z. Yue, Q. Zhang, Q. Zhang, X.-E. Zhang, Y. Zhao, X. Zhou and W. J. Parak, *ACS Nano*, 2017, **11**, 2313.

5 J. Xie, S. Lee and X. Chen, *Adv. Drug Delivery Rev.*, 2010, **62**, 1064.

6 R. Tong and D. S. Kohane, *Annu. Rev. Pharmacol. Toxicol.*, 2016, **56**, 41.

7 R. K. Thapa, Y. S. Youn, J.-H. Jeong, H.-G. Choi, C. S. Yong and J. O. Kim, *Colloids Surf., B*, 2016, **143**, 271.

8 R. S. Riley and E. S. Day, *Wiley Interdiscip. Rev.: Nanomed. Nanobiotechnol.*, 2017, **9**, e1449.

9 W.-J. Yin, Y.-P. Chen, Y.-E. Xie, L.-M. Liu and S. B. Zhang, *Phys. Chem. Chem. Phys.*, 2015, **17**, 14083–14087.

10 G. Modugno, C. Ménard-Moyon, M. Prato and A. Bianco, *Br. J. Pharmacol.*, 2015, **172**, 975.

11 P. T. Yin, S. Shah, M. Chhowalla and K.-B. Lee, *Chem. Rev.*, 2015, **115**, 2483.

12 C. Wang, J. Li, C. Amatore, Y. Chen, H. Jiang and X.-M. Wang, *Angew. Chem., Int. Ed.*, 2011, **50**, 11644.

13 J. Song, X. Yang, O. Jacobson, L. Lin, P. Huang, G. Niu, Q. Ma and X. Chen, *ACS Nano*, 2015, **9**, 9199.

14 Y. Zhang, C. Y. Ang and Y. Zhao, *Polym. J.*, 2016, **48**, 589.

15 A. B. S. Bakhtiari, D. Hsiao, G. Jin, B. D. Gates and N. R. Branda, *Angew. Chem., Int. Ed.*, 2009, **48**, 4166.

16 Y. Zhong, C. Wang, R. Cheng, L. Cheng, F. Meng, Z. Liu and Z. Zhong, *J. Controlled Release*, 2014, **195**, 63.

17 L. He, S. Sarkar, A. Barras, R. Boukherroub, S. Szunerits and D. Mandler, *Chem. Commun.*, 2017, **53**, 4022.

18 J. Taylor, A. Huefner, L. Li, J. Wingfield and S. Mahajan, *Analyst*, 2016, **141**, 5037.

19 S. Salatin and A. Yari Khosroushahi, *J. Cell. Mol. Med.*, 2017, **21**, 1668.

20 M. I. Setyawati, C. Y. Tay, D. Docter, R. H. Stauber and D. T. Leong, *Chem. Soc. Rev.*, 2015, **44**, 8174.

21 C. Saraiva, C. Praça, R. Ferreira, T. Santos, L. Ferreira and L. Bernardino, *J. Controlled Release*, 2016, **235**, 34.

22 S. Mishra, P. Webster and M. E. Davis, *Eur. J. Cell Biol.*, 2004, **83**, 97.

23 B. Romberg, W. E. Hennink and G. Storm, *Pharm. Res.*, 2008, **25**, 55.

24 A. Som, S. Bloch, J. E. Ippolito and S. Achilefu, *Sci. Rep.*, 2016, **6**, 27803.

25 M. Anderson, A. Moshnikova, D. M. Engelman, Y. K. Reshetnyak and O. A. Andreev, *Proc. Natl. Acad. Sci. U. S. A.*, 2016, **113**, 8177.

26 G. Bajaj, W. G. Van Alstine and Y. Yeo, *PLoS One*, 2012, **7**, e30899.

27 P. Xu, G. Bajaj, T. Shugg, W. G. Van Alstine and Y. Yeo, *Biomacromolecules*, 2010, **11**, 2352.

28 J. H. Byeon and Y.-W. Kim, *Chem. Eng. J.*, 2013, **229**, 540.

29 J. H. Byeon, A. Kulkarni, H.-K. Kim, D. H. Thompson and J. T. Roberts, *Biomacromolecules*, 2014, **15**, 2320.

30 R. K. Thapa, J. H. Byeon, S. K. Ku, C. S. Yong and J. O. Kim, *NPG Asia Mater.*, 2017, **9**, e416.

31 R. K. Thapa, J. Y. Choi, B. K. Poudel, H.-G. Choi, C. S. Yong and J. O. Kim, *Int. J. Nanomed.*, 2016, **11**, 2799.

32 R. Torres-Mendieta, D. Ventura-Espinosa, S. Sabater, J. Lancis, G. Mínguez-Vega and J. A. Mata, *Sci. Rep.*, 2016, **6**, 30478.

33 S. Bhandari, M. Deepa, A. G. Joshi, A. P. Saxena and A. K. Srivastava, *Nanoscale Res. Lett.*, 2011, **6**, 424.

34 J. Y. Choi, R. K. Thapa, C. S. Yong and J. O. Kim, *J. Pharm. Invest.*, 2016, **46**, 325.

35 R. K. Thapa, J. Y. Choi, B. Gupta, T. Ramasamy, B. K. Poudel, S. K. Ku, Y. S. Youn, H. G. Choi, C. S. Yong and J. O. Kim, *Biomater. Sci.*, 2016, **4**, 1340.

36 H. J. Shen, H. Shi, K. Ma, M. Xie, L. L. Tang, S. Shen, B. Li, X. S. Wang and Y. Jin, *Acta Biomater.*, 2013, **9**, 6123.

37 Y. A. Cheon, J. H. Bae and B. G. Chung, *Langmuir*, 2016, **32**, 2731.

38 Z. Sheng, L. Song, J. Zheng, D. Hu, M. He, M. Zheng, G. Gao, P. Gong, P. Zhang, Y. Ma and L. Cai, *Biomaterials*, 2013, **34**, 5236.

39 J. Peng, T. Qi, J. Liao, B. Chu, Q. Yang, Y. Qu, W. Li, H. Li, F. Luo and Z. Qian, *Theranostics*, 2014, **4**, 678.

40 C. F. Thorn, C. Oshiro, S. Marsh, T. Hernandez-Boussard, H. McLeod, T. E. Klein and R. B. Altman, *Pharmacogenet. Genomics*, 2011, **21**, 440.

41 E. L. Deer, J. Gonzalez-Hernandez, J. D. Coursen, J. E. Shea, J. Ngatia, C. L. Scaife, M. A. Firpo and S. J. Mulvihill, *Pancreas*, 2010, **39**, 425.

42 L. C. Davies, S. J. Jenkins, J. E. Allen and P. R. Taylor, *Nat. Immunol.*, 2013, **14**, 986.

43 M. Nikfarjam, V. Muralidharan and C. Christophi, *J. Surg. Res.*, 2005, **127**, 208.

44 C. Brace, *IEEE Pulse*, 2011, **2**, 28.

45 A. D. Hanna, A. Lam, S. Tham, A. F. Dulhunty and N. A. Beard, *Mol. Pharmacol.*, 2014, **86**, 438.

46 H. Lee, Y. Lee, C. Song, H. R. Cho, R. Ghaffari, T. K. Choi, K. H. Kim, Y. B. Lee, D. Ling, H. Lee, S. J. Yu, S. H. Choi, T. Hyeon and D. H. Kim, *Nat. Commun.*, 2015, **6**, 10059.